

# Genome-wide DNA-methylation profiles in human bone marrow mesenchymal stem cells on titanium surfaces

Mingyue Lyu<sup>1</sup>, Yunfei Zheng<sup>2</sup>,  
Lingfei Jia<sup>3</sup>, Yan Zheng<sup>1</sup>, Yanping  
Liu<sup>1</sup>, Ye Lin<sup>1</sup> , Ping Di<sup>1</sup>

<sup>1</sup>Department of Implantology, Peking University School and Hospital of Stomatology, Beijing; <sup>2</sup>Department of Orthodontics, Peking University School and Hospital of Stomatology, Beijing; <sup>3</sup>Department of Central Laboratory, Peking University School and Hospital of Stomatology, Beijing, China

Lyu M, Zheng Y, Jia L, Zheng Y, Liu Y, Lin Y, Di P. Genome-wide DNA-methylation profiles in human bone marrow mesenchymal stem cells on titanium surfaces.

*Eur J Oral Sci* 2019; 127: 196–209. © 2019 Eur J Oral Sci

The characteristics of titanium (Ti) have been shown to influence dental implant fixation. Treatment of surfaces using the sandblasted, large-grit, acid-etched (SLA) method is widely used to provide effective osseointegration. However, the DNA methylation-associated mechanism by which SLA surface treatment affects osseointegration of human bone marrow mesenchymal stem cells (hBMSCs) remains elusive. Genome-wide methylation profiling of hBMSCs on SLA-treated and machined smooth Ti was performed using Illumina Infinium Methylation EPIC BeadChip at day 7 of osteogenic induction. In total, 2,846 CpG sites were differentially methylated in the SLA group compared with the machined group. Of these sites, 1,651 (covering 1,066 genes) were significantly hypermethylated and 1,195 (covering 775 genes) were significantly hypomethylated. Thirty significant enrichment pathways were observed, with Wnt signaling being the most significant. mRNA expression was identified by microarray and combined with DNA-methylation profiles. Thirty-seven genes displayed negative association between mRNA expression and DNA-methylation level, with the osteogenesis-related genes insulin-like growth factor 2 (*IGF2*) and carboxypeptidase X, M14 Family Member 2 (*CPXM2*) showing significant up-regulation and down-regulation, respectively. In summary, our results demonstrate differences between SLA-treated and machined surfaces in their effects on genome-wide DNA methylation and enrichment of osteogenic pathways in hBMSCs. We provide novel insights into genes and pathways affected by SLA treatment in hBMSCs at the molecular level.

Ye Lin, Department of Oral Implantology, Peking University School and Hospital of Stomatology, 22 Zhongguancun Avenue South, Haidian District, Beijing 100081, China

E-mail: yorcklin@263.net

Key words: epigenetics; microarray; osteogenic differentiation; sandblasted, large-grit and acid-etched (SLA)

Accepted for publication December 2018

The clinical success of titanium (Ti) implants is associated with their early osseointegration (1, 2). Physical and chemical characteristics of the implant surface influence osseointegration, a complicated biological process containing immunoinflammatory responses, angiogenesis, and osteogenesis (1–3). The surface roughness of Ti is a key factor in regulating osteogenic cell responses during dental implant healing (4–6). Individual studies and reviews have documented that high implant success rates depend on the implant surface characteristics, with roughened implant surfaces providing higher success rates than implants with relatively smoother surfaces (7–10).

Sandblasting with large grit followed by acid etching (SLA) is a treatment widely used for implants and has been shown to provide effective osseointegration in many studies (2, 10, 11). According to one systematic review, SLA-treated surfaces are often compared with machined surfaces and the former are usually found to

be more strongly integrated into bone (12). Compared with machined Ti surfaces, SLA-treated Ti implants with a relatively rough surface have been found to enhance bone-to-implant shear strength and bone apposition in histomorphometric analyses (13, 14). However, the underlying mechanism by which SLA treatment affects osseointegration remains elusive.

Bone marrow mesenchymal stem cells (BMSCs) are multipotent cells that can differentiate into skeletal cell types, including osteoblasts, chondrocytes, adipocytes, fibroblasts, and adventitial reticular cells (15). Bone marrow mesenchymal stem cells are implicated in early tissue-implant interactions that result in formation of osteoblasts to establish osseointegration, and they are crucial for bone remodeling around implants (16, 17). Bone marrow mesenchymal stem cells can modulate osseointegration through the expression of various genes regulated at epigenetic, translational, and post-translational levels (18, 19). Epigenetic regulation, such

as histone modification and DNA methylation, plays an important role in regulating gene expression (20, 21). The aberrant methylation of CpG islands in the promoter or first exon silences the genes by modifying the accessibility of the DNA to the transcriptional machinery (22, 23). Current studies indicate that hypermethylation of CpG islands induces osteogenic differentiation of human bone marrow mesenchymal stem cells (hBMSCs) (2). A recent study states that the DNA-methylation profile is associated with the osteogenic potential of three distinct types of human odontogenic stem cells (24). Thus, comparative genome-wide DNA-methylation analysis is a powerful tool for studying methylation changes associated with osteogenic differentiation of stem cells (2, 25). The Illumina Infinium Methylation 450 BeadChip is widely used for assessing epigenetic changes covering 485,764 CpG sites (26, 27), and an advanced chip platform to validate the specific stem cell types and reveal precise details of DNA-methylation profiles is required.

Currently, no genome-wide DNA-methylation profiling or integrated analysis between DNA methylation and mRNA expression in hBMSCs cultured on Ti has been conducted (28). In this study, we determined the DNA-methylation patterns of hBMSCs seeded onto SLA-treated Ti. Bioinformatic analysis was performed to identify potential target genes and pathways. This study provides insight into the precise mechanism of osseointegration on SLA-treated surfaces.

## Material and methods

### Preparation of Ti specimens

Titanium specimens were divided into two groups: the SLA group (positive control); and the machined smooth group (negative control). All pure Ti slices (99.6% purity; Weigao, Weihai, China) were polished with silicon carbide sandpaper and washed with acetone, absolute alcohol, and deionized water (dH<sub>2</sub>O) in an ultrasonic cleaner for 15 min. Subsequently, the specimens were dried at room temperature for 1 h. The SLA groups were further processed as follows: each Ti slice was sandblasted by aluminium oxide (Al<sub>2</sub>O<sub>3</sub>) particles, 0.25–0.5 mm in diameter. Subsequently, the specimens were etched using a mixture of hydrogen fluoride (HF) and nitric acid (HNO<sub>3</sub>) at room temperature for 10 min, and then in a mixture of hydrogen chloride (HCl) and sulfuric acid (H<sub>2</sub>SO<sub>4</sub>) at 60°C for 30 min. The Ti specimens were cleaned ultrasonically in dH<sub>2</sub>O for 15 min. All specimens were sterilized in an autoclave (120°C for 30 min) before use in the in-vitro experiments. We prepared Ti slices of different diameters. Slices with diameter of 3.5 cm fit the 6-well plates and those with diameter of 1.5 cm fit the 24-well plates.

### Surface characterization

The surface topography of the machined smooth and SLA-treated Ti surfaces were characterized using a scanning electron microscope (Hitachi, Tokyo, Japan). The surface roughness was examined using a 3D Optical

Microscope (CountourGT-K; Bruker, Tucson, AZ, USA). The measurements were conducted under contact mode in dry conditions.

### hBMSCs culture and osteogenic induction

Human bone marrow mesenchymal stem cells were purchased from ScienCell (San Diego, CA, USA). All materials were purchased from Sigma-Aldrich (St Louis, MO, USA) unless otherwise stated. Dulbecco's modified Eagle's medium (DMEM), fetal bovine serum (FBS), and 100× penicillin and streptomycin mixture were purchased from Gibco (Grand Island, NY, USA). Human bone marrow mesenchymal stem cells were cultured in fresh DMEM containing 10% (v/v) FBS, 100 U ml<sup>-1</sup> of penicillin G, and 100 mg ml<sup>-1</sup> of streptomycin at 37°C in an incubator with an atmosphere consisting of 5% CO<sub>2</sub> and 100% relative humidity. All in-vitro experiments were repeated three times using hBMSCs. Osteogenic-inducing medium, composed of fresh DMEM containing 10% (v/v) FBS, 100 U ml<sup>-1</sup> of penicillin G and 100 mg ml<sup>-1</sup> of streptomycin, 10 nM dexamethasone, 10 mM β-glycerophosphate, and 50 mg ml<sup>-1</sup> of L-ascorbic acid, was purchased from Cyagen Biosciences (Santa Clara, CA, USA). Human bone marrow mesenchymal stem cells were seeded at 1.0 × 10<sup>4</sup> cells cm<sup>-2</sup> on the SLA-treated and machined smooth Ti specimens. Cell solution was added into a blank well with no Ti slice to observe the density of the cells under a light microscope.

### Immunofluorescence

Human bone marrow mesenchymal stem cells were seeded in 6-well plates at 1.0 × 10<sup>4</sup> cells cm<sup>-2</sup> and divided into two groups (SLA-treated and machined smooth Ti surfaces) after osteogenic induction (OI) for 7 d. The hBMSCs were soaked in paraformaldehyde for 20 min, serially washed in PBS, and permeabilized with 0.5% Triton X-100 for 5 min. Then, the hBMSCs were serially washed in PBS and immunostained at room temperature for 1 h with antibodies against F-Actin (Sigma-Aldrich). Afterwards, the cells were again serially washed in PBS before counterstaining with DAPI (Solarbio, Beijing, China) at 37°C for 10 min. The fluorescence signal was observed and imaged using a confocal laser-scanning microscope LSM710 (Carl Zeiss, Oberkochen, Germany).

### Alkaline phosphatase activity

Human bone marrow mesenchymal stem cells were seeded in 24-well plates at 1.0 × 10<sup>4</sup> cells cm<sup>-2</sup> and divided into two groups (SLA-treated Ti and smooth Ti surfaces) after osteoinduction for 7 d. Alkaline phosphatase (ALP) activity was determined by staining with nitro blue tetrazolium (NBT) and 5-bromo-4-chloro-3-indolyl phosphate (BCIP), after osteoinduction for 7 d, using an ALP kit (CoWin Biosciences, Beijing, China). Briefly, cells were washed with PBS, treated with 4% formaldehyde for fixation, and washed with PBS again. Cells were stained with staining solution consisting of BCIP, NBT, and NBT buffer (1:1:38; vol/vol/vol). After washing several times with dH<sub>2</sub>O, specimens were observed and photographed with a stereomicroscope (Leica, M125; Wetzlar, Hesse, Germany). The intensities of the images were quantified using IMAGEJ software (<http://rsb.info.nih.gov/ij/>).

### RNA extraction, reverse transcription, and quantitative real-time PCR

Human bone marrow mesenchymal stem cells were seeded at a density of  $1.0 \times 10^4$  cells  $\text{cm}^{-2}$  on the SLA-treated Ti and smooth Ti specimens in 6-well plates, and RNA was isolated at 0 and 7 d of osteoinduction. Total cellular RNA was isolated after osteoinduction over a period of 7 d using the TRIzol reagent (Invitrogen, Carlsbad, CA, USA). First-strand cDNA synthesis was performed using the Reverse Transcription System from Promega (Madison, WI, USA). Quantification of all gene transcripts was performed by real-time PCR (qPCR) using a Power SYBR Green PCR Master Mix and an ABI PRISM 7500 sequence detection system (BGI, Shenzhen, China). Expression of glyceraldehyde-3-phosphate (*GAPDH*) was used as the internal control. The primers used were: osteocalcin (*OCN*), (forward) 5'-CAC TCC CCC TAT TGG C-3' and (reverse) 5'-CCC TCC TGC TTG GAC ACA AAG-3'; *GAPDH*, (forward) 5'-AAC TTT GGC ATT GTG GAA GG-3' and (reverse) 5'-ACA CAT TGG GGG TAG GAA CA-3'; and osterix (*OSX*), (forward) 5'-CCT CTG CGG GAC TCA ACA AC-3' and (reverse) 5'-TAA AGG GGG CTG GAT AAG CAT-3'. The cycle threshold values ( $C_t$  values) were used to calculate fold differences using the  $\Delta\Delta C_t$  method.

### Western blotting

Human bone marrow mesenchymal stem cells were seeded at a density of  $1.0 \times 10^4$  cells  $\text{cm}^{-2}$  on SLA-treated Ti and smooth Ti specimens in 6-well plates. Cells were lysed in RIPA lysis buffer [50 mM Tris-HCl, pH 8.0, 250 mM NaCl, 1% Nonidet P-40 (NP40), 0.5% (w/v) sodium deoxycholate and 0.1% SDS] at 7 d of osteoinduction. Lysates were sonicated and centrifuged at 12,000 r.p.m. (11,300 g) at 4°C for 10 min. The supernatant was collected and stored at 80°C until use. Aliquots (20  $\mu\text{g}$ ) of the protein extracts were subjected to electrophoresis through a 12% SDS-polyacrylamide gel and transferred to polyvinylidene difluoride membrane (Millipore, Cambridge, MA, USA). After blocking, proteins were detected by overnight incubation with primary antibodies against OSX (Affinity Bioscience, Cincinnati, OH, USA), OCN (Abcam, Cambridge, UK), and GAPDH (Sungene Biotech, Tianjin, China, 1:10,000 dilution) at dilutions of 1:1,000. After washing, the membranes were incubated with secondary antibodies (Zhongshan Goldenbridge, Beijing, China, 1:10,000 dilution) at room temperature for 1 h. The specific complexes were visualized using an ECL Kit (Applygen, Beijing, China).

### RNA and DNA isolation and microarray analysis

Human bone marrow mesenchymal stem cells were seeded at a density of  $1.0 \times 10^4$  cells  $\text{cm}^{-2}$  on the SLA-treated Ti and smooth Ti specimens in 6-well plates. RNA and DNA were isolated at 0 and 7 d of osteoinduction. DNA was isolated from cells on 4–6 pieces of SLA-treated Ti specimens and 4–6 pieces of smooth Ti specimens, separately, using phenol-chloroform extraction and an ultrasonic purification method. Subsequently, the EZ DNA Methylation-Gold kit (Zymo Research, Irvine, CA, USA) was used for bisulfite conversion of DNA. Bisulfite converted DNA was thereafter hybridized to the Illumina Infinium Methylation EPIC Bead Chip, representing the

methylation state of over 850 K CpG sites. The array was imaged using the Illumina iScan system (Illumina, San Diego, CA, USA) in which the percent methylation of each CpG site was quantified for the entire study group. The Illumina 850 K Methylation Bead Chip provides unparalleled genome-wide coverage featuring the guidance of methylation experts. The experiments (DNA and RNA extraction and microarray analysis) were all performed in the Laboratory of Capital Bio Corporation (Beijing, China).

Total RNA was extracted from samples using TRIzol reagent, according to the manufacturer's instructions, and quantified using a Nano Drop ND-1000 spectrophotometer (Thermo Scientific, Wilmington, DE, USA). RNA integrity was determined with 1% formaldehyde denaturing agarose gel electrophoresis. Pure RNA samples (absorbance: 260/280  $\geq 1.8$ ) and with an integrity RNA ratio (28S/18S)  $\geq 1.5$  were used in further microarray experiments. Message RNA expression profiling was performed using lncRNA & mRNA Human Gene Expression Microarray V4.0 in the Laboratory of Capital Bio Corporation, according to the manufacturer's instructions. The Agilent human lncRNA and mRNA array V4.0 was designed with four identical arrays per slide (180 K format), with each array containing probes interrogating approximately 41,000 and 34,000 human lncRNAs and mRNAs, respectively.

### Data processing

The raw files were processed for quality control and normalization. The signal intensity of each methylation locus was obtained using GENOME STUDIO software version 1.1.0 (Illumina). The methylation value was calculated through the different types of probes by fluorescence, deviation correction, and normalization. The methylation level of a locus was measured as beta ( $\beta$ ) =  $M/(M + U)$ , where  $M$  represents the methylated signals and  $U$  represents the unmethylated signals. The  $\beta$  value ranges continuously from 0 (unmethylated) to 1 (fully methylated). Furthermore, we corrected and normalized the deviation caused by different fluorescent markers and probes. Finally, we obtained the methylation level of each tested site as a  $\beta$ -value.

mRNA expression data were extracted using Agilent Feature Extraction (V10.7) from Agilent Technologies (Santa Clara, CA, USA) and summarized, normalized, and controlled for quality using Gene Spring (V13.0) from Agilent Technologies. Then, log<sub>2</sub> transformation was applied to the data using the Adjust Data function of MULTI-EXPERIMENT VIEWER (MEV) software (Cancer Computational Biology at Dana-Farber Cancer Institute, Boston, MA, USA; <http://mev.tm4.org/#/welcome>). Subsequently, after further filtering out probes with a sample detection rate of <20%, or without gene annotation information, R package (<https://www.r-project.org/>) was used to select the probe ID with the largest interquartile range (IQR) of expression values to represent the gene (29).

### Statistical analysis

The Empirical Bayes moderated  $t$  test of the limma package from Bioconductor (Bioconductor online: <https://www.bioconductor.org/>) was used to compare the methylation profile difference between the SLA-treated group and the control group. For multiple testing, the  $P$  value was corrected using Benjamini-Hochberg tests at 5% false discovery rate (FDR) (30). For quality control, the CpG

sites with missing values or detection  $P > 0.05$  in more than 90% of specimens were eliminated. The CpG sites with both adjusted  $P \leq 0.05$  and  $|\beta \text{ difference}| \geq 0.10$  were identified as significantly differentially methylated loci.

The mRNA array data were analyzed for data summarization, normalization, and quality control using GENE SPRING software V13.0 (Agilent). To select differentially expressed genes, we used threshold values of  $\geq 2$  and  $\leq -2$ -fold change and a  $t$ -test  $P$  value of 0.05. The data were log2 transformed and median centered by genes using the Adjust Data function of CLUSTER 3.0 software (Michael Eisen, Stanford University, Stanford, CA, USA; <http://bonsai.hgc.jp/~mdehoon/software/cluster/software.htm>), then further analyzed using hierarchical clustering with average linkage (26). Finally, we performed tree visualization using Java Tree view (Stanford University School of Medicine, Stanford, CA, USA).

### Integrated analysis of DNA methylation and mRNA expression

To identify DNA-methylation changes with concomitant changes in gene expression, we combined the gene-expression profiles and DNA-methylation profiles of the SLA group with the control.

### Gene ontology, pathway, and disease enrichment analyses

Gene ontology (GO) and pathway enrichment analyses were conducted using DAVID (<http://david.abcc.ncifcrf.gov/>) with all genes and pathways available on the Illumina Infinium Methylation 850 BeadChip platform and the lncRNA & mRNA Human Gene Expression Microarray V4.0 (CapitalBio Corporation, Beijing, China). Molecular function (MF), cellular component (CC), and biologic process (BP) were considered for GO enrichment analysis. For pathway and disease enrichment analysis, we employed KEGG PATHWAY and KEGG DISEASE (<http://www.genome.jp/kegg/>) in this study. The GO terms, pathways, and diseases were considered significantly enriched with FDR-adjusted  $P \leq 0.05$ .

## Results

### Surface characterization

The morphologies of SLA-treated and machined smooth Ti were characterized by scanning electron microscopy (Fig. 1A). The SLA-treated Ti surface (right column) exhibited higher roughness compared with the machined smooth Ti surface (left column). Multi-level pores were observed on the roughened surfaces. Microscopic evaluation demonstrated that each pit with diameter of about 0–50  $\mu\text{m}$  contained several micro-pits with diameters of 0.5–2  $\mu\text{m}$ . The average Ra value of the SLA-treated Ti surface is 1.8  $\mu\text{m}$ , and that of the smooth Ti surface is 0.2  $\mu\text{m}$ .

### Immunofluorescence analysis

We used immunofluorescence to observe cell morphology on machined smooth and SLA-treated Ti surfaces on days 0 (Fig. 1B) and 7 (Fig. 1C,D). Phalloidin was used to

detect F-Actin, and hBMSCs showed similar morphology on both SLA-treated surfaces and smooth surfaces on day 0. As shown in Fig. 1C,D, spindle cells were observed and spread out in one orientation on smooth Ti surfaces, while, on the SLA-treated Ti surfaces, cells extended to a larger polygonal morphology. Cells spread extensively with pseudopodia and interwove on SLA-treated Ti surfaces.

### Osteogenic differentiation of hBMSCs on different Ti surfaces

As shown in Fig. 2A,B, on day 7 of osteoinduction, the cells on SLA-treated Ti surfaces exhibited more pronounced areas of ALP staining compared with cells on machined smooth Ti surfaces. The results quantified using IMAGEJ software showed that, compared with the control group, ALP activities were significantly increased in the SLA-treated group (Fig. 2C).

Gene and protein expression of *OCN* and *OSX* were detected. After 7 d of osteoinduction, the relative expression of *OCN* and *OSX* in hBMSCs on the SLA-treated Ti surface was significantly higher than that on the smooth Ti surface, as determined by RT-qPCR (Fig. 2D,E) and western blotting (Fig. 2F).

### Identification of differentially methylated loci

Figure 3A represents the heatmap for genome-wide methylation profiles. Hypermethylated sites (shown in dark red) were more widespread in the SLA-treated group than in the machined smooth group. However, hypomethylated sites (shown in dark green) were more prevalent in the machined smooth group, suggesting that a larger number of gene promoters in hBMSCs on the SLA-treated Ti surface, than on the machined smooth Ti surface, are hypermethylated.

Notably, we also found that 236 sites are located in CpG islands (Fig. 3B). A total of 845,636 CpG sites passing the quality control procedure were analyzed in this study. At the CpG site level, we detected 2,846 significantly differentially methylated sites, including 1,651 hypermethylated loci and 1,195 hypomethylated loci in the SLA-treated group compared with controls (Fig. 3C), at a 5% FDR. At the gene level, 1,066 hypermethylated genes and 775 hypomethylated genes were mapped (Fig. 3D). Eight genes [cytochrome P450 family 2 subfamily W member 1 (*CYP2W1*), plectin (*PLEC1*), mitochondrial ribosomal protein S21 (*MRPS21*), protein kinase C theta (*PRKCQ*), calcium binding and coiled-coil domain 1 (*CALCOCO1*), aldehyde dehydrogenase 1 family member A1 (*ALDH1A1*), Rho GTPase activating protein 24 (*ARHGAP24*), myocyte enhancer factor 2D (*MEF2D*)] correspond to the 10 most hypomethylated CpG sites in the SLA-treated group, as shown in Table 1. Another seven genes [C-terminal binding protein 1 (*CTBP1*), GRB2 binding adaptor protein, transmembrane (GAPT), MAP3K7 C-terminal like (*MAP3K7CL*), cation channel sperm associated auxiliary subunit gamma (*CATSPERG*), sodium voltage-gated channel beta subunit 4 (*SCN4B*), ubiquitin specific peptidase 34 (*USP34*), autophagy and beclin 1 regulator 1 (*AMBRA1*)]

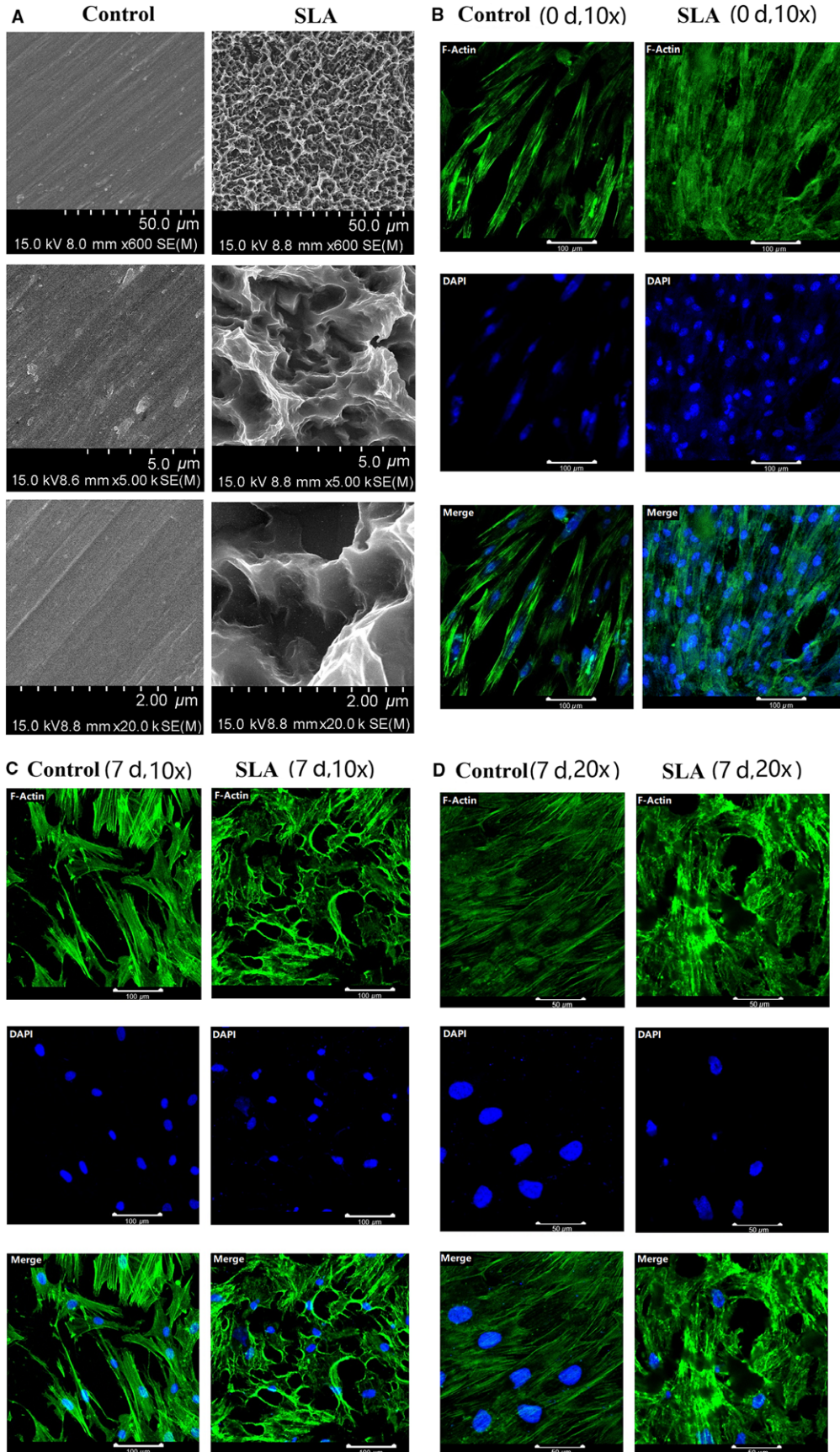


Fig. 1. (A) Characterization, at different magnifications, of the machined smooth titanium surface (control) (left column) and the sandblasted, large-grit, acid-etched (SLA)-treated titanium surface (right column) by scanning electron microscopy. (B) Representative immunofluorescence images showing expression of F-Actin in control (left column) and SLA (right column) groups at 0 d. Antibodies are shown in green and nuclei are shown in blue. Scale bar = 100  $\mu\text{m}$ . (C, D) Representative immunofluorescence images showing expression of F-Actin in control (left) and SLA (right) groups at 7 d at different magnifications. Antibodies are shown in green and nuclei are shown in blue. Scale bars = 100  $\mu\text{m}$  (C) and 50  $\mu\text{m}$  (D).

correspond to the 10 most hypermethylated CpG sites in the SLA-treated group (Table 2). The CpG sites with both adjusted  $P \leq 0.05$  and  $|\beta \text{ difference}| \geq 0.10$  were identified as significantly differentially methylated loci. These data imply that the gene promoters are prone to be methylated when hBMSCs are grown on SLA-treated Ti.

### Methylation site-based GO, pathway, and disease enrichment analyses

We identified GO terms significantly enriched in the differentially methylated genes. In the SLA-treated group, genes involved in osteogenic activities, such as cell adhesion, cell differentiation, cytoskeletal organization, beta-catenin binding, and MAPK kinase activity, were up-regulated (Fig. 4A,B). As presented in Fig. 4C, pathway enrichment analysis detected 30 pathways with differentially methylated genes for the SLA-treated group ( $P \leq 0.05$ ), with the Wnt signaling and cadherin signaling pathways being the most significant. We identified disease terms significantly enriched in the differentially methylated genes (Fig. 4D).

Genes involved in Type 2 diabetes and obesity-related traits were significantly up-regulated in the SLA-treated group. These results suggest that the genes involved in osteogenic GO activities and pathways were hypomethylated in hBMSCs grown on SLA-treated Ti compared with hBMSCs grown on machined smooth Ti.

### Analysis of mRNA transcriptome, GO, and pathway enrichment

Microarray analysis using an lncRNA & mRNA Human Gene Expression Microarray V4.0 was performed after osteoinduction for 7 d.

Figure 5A represents the heatmap from genome-wide mRNA profiles. About 25,654 mRNAs were detected. Differential expression analysis showed that 366 genes were up-regulated and 316 genes were down-regulated (Fig. 5B).

In the SLA-treated group, genes involved in extracellular matrix (ECM) organization, ECM structure organization, collagen binding, and calcium ion binding GO activities were up-regulated (Fig. 6A,B). Genes involved

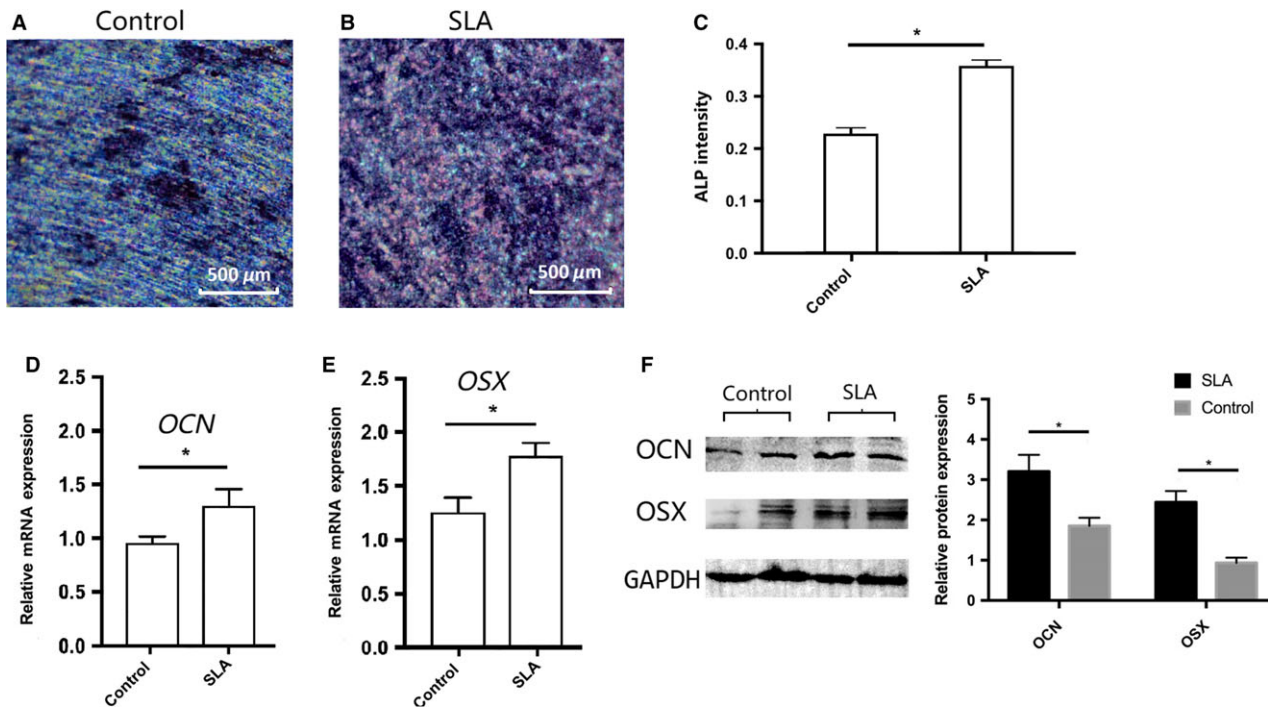
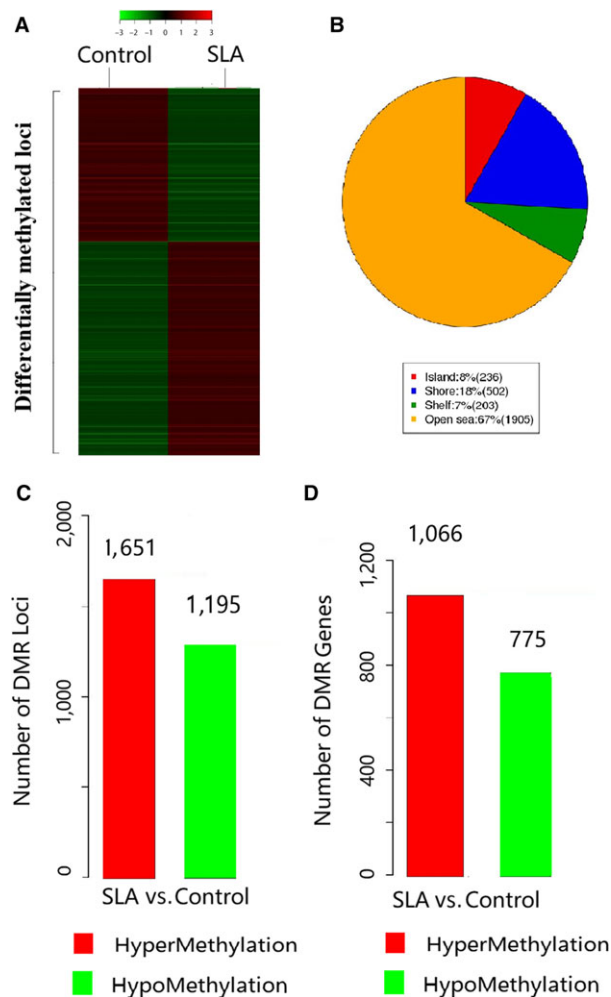


Fig. 2. The sandblasted, large-grit, acid-etched (SLA)-treated titanium surface promotes osteogenic differentiation of human bone marrow mesenchymal stem cells (hBMSCs) in vitro at 7 d. (A) Alkaline phosphatase (ALP) staining of hBMSCs cultured on a machined smooth titanium surface (control). (B) ALP staining of hBMSCs cultured on an SLA-treated titanium surface. (C) Histograms show quantification of the image intensities obtained by ALP staining. (D) RT-qPCR analysis of osteocalcin (OCN) expression in control and SLA groups. (E) qRT-PCR analysis of osterix (OSX) expression in control and SLA groups. (F) Western blotting (left) and quantification (right) of expression of OCN, OSX, and the internal control, glyceraldehyde-3-phosphate dehydrogenase (GAPDH) at the indicated time points. Results are given as mean  $\pm$  SD ( $*P < 0.05$ ).



**Fig. 3.** DNA methylation in human bone marrow mesenchymal stem cells (hBMSCs) cultured on sandblasted, large-grit, acid-etched (SLA)-treated titanium is significantly different from that in hBMSCs cultured on machined smooth titanium, at 7 d. (A) Heat map of hierarchical clustering analysis represents DNA-methylation levels from completely methylated (red) to unmethylated (green). (B) Distribution of genomic regions for all significantly differentially methylated CpG sites in hBMSCs on SLA-treated titanium compared with machined smooth titanium. (C) Number of hypomethylated or hypermethylated CpG sites. (D) Number of hypomethylated or hypermethylated genes.  $|\Delta\beta\text{-value}| \geq 0.1$ ,  $P \leq 0.05$ , false discovery rate (FDR) (Adjusted  $P$  value)  $\leq 0.05$ .

in osteogenic pathways, including ECM–receptor interaction, the phosphoinositide 3-kinase (PI3K)–Akt signal pathway, and mineral absorption, were up-regulated (Fig. 6C). In summary, these results showed that the differentially expressed genes involved in osteogenic GO activities and pathways were up-regulated in hBMSCs grown on SLA-treated Ti compared with hBMSCs grown on machined smooth Ti.

#### Integrated analysis of DNA methylation and mRNA expression

It is well established that changes in DNA methylation and differences in gene regulation are causally related,

with hypomethylation generally leading to gene expression and hypermethylation resulting in gene silencing (30). A total of 37 genes with 54 methylated probes were inversely correlated with changes in expression. Significantly hypomethylated CpG sites corresponded to up-regulation of the gene *INS-IGF2* readthrough (*INS-IGF2*) and significantly hypermethylated CpG sites corresponded to down-regulation of the gene carboxypeptidase X, M14 Family Member 2 (*CPXM2*) in hBMSCs on SLA-treated Ti compared with machined smooth Ti, as shown in Table 3. The CpG sites with both adjusted  $P \leq 0.05$  and  $|\beta$  difference|  $\geq 0.10$  were identified as significantly differentially methylated loci. In the SLA-treated group, genes involved in MAP kinase phosphatase, cell differentiation, and cytoskeletal protein binding were up-regulated (Fig. 7A). Genes involved in osteogenic pathways, including cell adhesion molecules, NF-kappa B signaling pathways, and apoptosis, were up-regulated (Fig. 7B).

#### Discussion

A combination of sandblasting and etching has been commonly used as a surface-modification technique; this technique is also widely used clinically, resulting in effective osseointegration (11). In our study, we prepared SLA-treated Ti slices with different diameters and characterized the surface. The surface topography is dependent on the surface orientation and roughness. The average Ra value of the SLA-treated surface is  $1.8 \mu\text{m}$ , while that of the smoothed surface is  $0.2 \mu\text{m}$ . Multi-level pores were also observed on SLA-treated surfaces. Compared with the machined surface, the SLA-treated surface had increased surface roughness and modified surface topography, resulting in a multi-level structure. The SLA procedure hypothetically achieves a roughness optimal for mechanical fixation, whereas additional etching smoothens out some sharp peaks (4, 12). The peaks may enhance potential protein adhesion on the implant surface, considered to be important for the early bone-healing process (12). Confocal microscopy photographs taken in this study show that cells spread extensively with pseudopodia and interweave on the SLA-treated surface.

Better and faster bone integration of SLA-treated implants in the initial healing period, as reported by several authors, may be caused by production of higher levels of local cytokines and growth factors (31). As demonstrated by researchers in an in vitro study with osteoblast-like cells, there was a direct relationship between transforming growth factor- $\beta 1$  (TGF- $\beta 1$ ) production and surface roughness, and prostaglandin E<sub>2</sub> (PGE<sub>2</sub>) content in the media of cultures grown on the roughest surfaces was significantly increased (by 1.5–4.0 times) compared with that for cultures grown on smooth surfaces (32). Mechanistically, the expression of these genes is regulated by epigenetics, including DNA methylation. Our data indicate that the topography of SLA-treated surfaces modifies the methylation level of DNA in cells that are cultured on such surfaces.

Table 1

Top 10 hypomethylated CpG sites and corresponding genes of human bone marrow mesenchymal stem cells (hBMSCs) cultured on sandblasted, large-grit, acid-etched (SLA)-treated titanium compared with machined smooth titanium, determined using the high-resolution Infinium 850 K methylation array

Target ID	Beta-Difference	Mean SLA DNA	Mean machined DNA	P-value	Adjust P-value	UCSC REFGENE NAME
cg04141948	-0.297	0.322	0.619	0.024	0.024	<i>CYP2W1</i>
cg13527203	-0.255	0.624	0.879	0.037	0.037	<i>PLEC1</i>
cg08293086	-0.205	0.184	0.389	0.013	0.013	<i>MRPS21</i>
cg03143269	-0.168	0.558	0.726	0.013	0.013	
cg03993163	-0.165	0.679	0.844	0.004	0.004	<i>PRKCQ</i>
cg06157435	-0.163	0.232	0.395	0.012	0.012	<i>CALCOCO1</i>
cg08867461	-0.161	0.359	0.52	0.023	0.023	<i>ALDH1A1</i>
cg01170806	-0.156	0.502	0.658	0.002	0.002	<i>ARHGAP24</i>
cg18266783	-0.147	0.382	0.529	0.046	0.047	<i>MEF2D</i>
cg20480497	-0.147	0.207	0.354	0.050	0.050	

The methylation level of a locus was measured as beta ( $\beta$ ) =  $M/(M + U)$ , where  $M$  was the methylated signals and  $U$  was the unmethylated signals. For a gene corresponding to a CpG site, Mean SLA DNA and Mean machined DNA represent the  $\beta$  value of the SLA group and machined smooth group, respectively. Beta-Difference equals the  $\beta$  value differences between the SLA group and machined smooth group. For multiple testing the Adjust  $P$  value was corrected by Benjamini–Hochberg tests at 5% false discovery rate (FDR). UCSC REFGENE NAME represents the gene symbol corresponding to the CpG site.

The CpG sites with both adjusted  $P \leq 0.05$  and  $|\beta$  difference|  $\geq 0.10$  were identified as significantly differentially methylated loci. *ALDH1A1*, aldehyde dehydrogenase 1 family member A1; *ARHGAP24*, Rho GTPase activating protein 24; *CALCOCO1*, calcium binding and coiled-coil domain 1; *CYP2W1*, cytochrome P450 family 2 subfamily W member 1; *MEF2D*, myocyte enhancer factor 2D; *MRPS21*, mitochondrial ribosomal protein S21; *PLEC1*, plectin; *PRKCQ*, protein kinase C theta.

Table 2

Top 10 hypermethylated CpG sites and corresponding genes of human bone marrow mesenchymal stem cells (hBMSCs) cultured on sandblasted, large-grit, acid-etched (SLA)-treated titanium compared with machined smooth titanium, determined using the high-resolution Infinium 850 K methylation array

Target ID	Beta-Difference	Mean SLA DNA	Mean machined DNA	P-value	Adjust P-value	UCSC REFGENE NAME
cg20890325	0.475	0.758	0.283	0.001	0.001	<i>CTBPI</i>
cg12491659	0.204	0.559	0.355	0.002	0.002	<i>GAPT</i>
cg20707156	0.171	0.495	0.324	0.001	0.001	
cg17280027	0.17	0.538	0.368	0.050	0.050	<i>MAP3K7CL</i>
cg09094448	0.166	0.372	0.206	0.037	0.037	<i>CATSPERG</i>
cg18926420	0.166	0.555	0.389	0.043	0.043	
cg20341535	0.162	0.584	0.422	0.028	0.028	<i>SCN4B</i>
cg01923102	0.158	0.376	0.218	0.016	0.016	<i>USP34</i>
cg17020421	0.147	0.469	0.322	0.016	0.016	
cg14416830	0.145	0.284	0.139	0.040	0.040	<i>AMBRA1</i>

The methylation level of a locus was measured as beta ( $\beta$ ) =  $M/(M + U)$ , where  $M$  represents the methylated signals and  $U$  represents the unmethylated signals. For a gene corresponding to a CpG site, Mean SLA DNA and Mean machined DNA represent the  $\beta$  value of SLA group and machined smooth group, respectively. Beta-Difference equals the  $\beta$  value differences between the SLA group and machined smooth group. For multiple testing the Adjust  $P$  value was corrected by Benjamini–Hochberg tests at 5% false discovery rate (FDR). UCSC REFGENE NAME represents the gene symbol corresponding to the CpG site.

The CpG sites with both adjusted  $P \leq 0.05$  and  $|\beta$  difference|  $\geq 0.10$  were identified as significantly differentially methylated loci. *AMBRA1*, autophagy and beclin 1 regulator 1; *CATSPERG*, cation channel sperm associated auxiliary subunit gamma; *CTBPI*, C-terminal binding protein 1; *GAPT*, GRB2 binding adaptor protein, transmembrane; *MAP3K7CL*, MAP3K7 C-terminal like; *SCN4B*, sodium voltage-gated channel beta subunit 4; *USP34*, ubiquitin specific peptidase 34.

Consistent with our study, the Ti nanotube was found to modify the chromatin status of human adipose-derived stem cells, thereby regulating the expression of osteogenesis-associated genes (33).

Numerous studies have reported that the initial bone formed around rough Ti implants occurs not only on the exposed bone wall of the surgically created implant bed but also vertically along the implant surface (34). In accordance, researchers have tried to develop

osteoconductive dental implant interfaces to improve and accelerate bone deposition (35). The characteristics of the material and further surface modifications may assist periosteal-derived cell proliferation and bone deposition (36). In this study, we identified differentially expressed genes in hBMSCs on SLA-treated and machined surfaces during the early stages of osteoblast differentiation. As initial bone formation also occurs on the implant surface, these differentially expressed genes

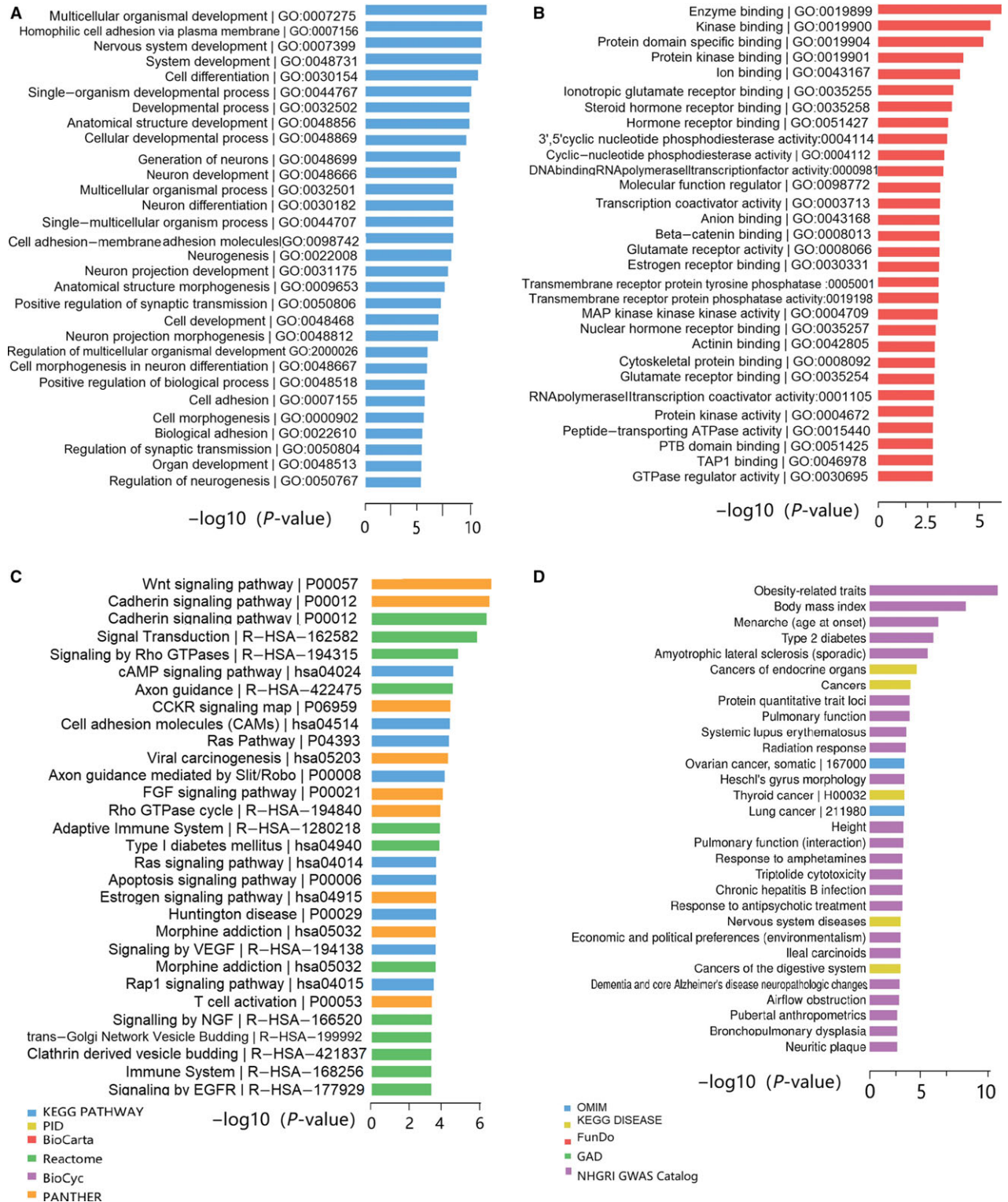


Fig. 4. Gene ontology (GO), KEGG pathway, and disease analysis of differentially methylated genes. (A) Summary of the GO analysis of the categories of 'Biological processes' among the differentially methylated genes. The GO category is listed on the y-axis. (B) Summary of the GO analysis of the categories of 'Cellular components' among the differentially methylated genes. The GO category is listed on the y-axis. (C) KEGG pathway analysis of the differentially methylated genes. (D) Disease analysis of the differentially methylated genes.

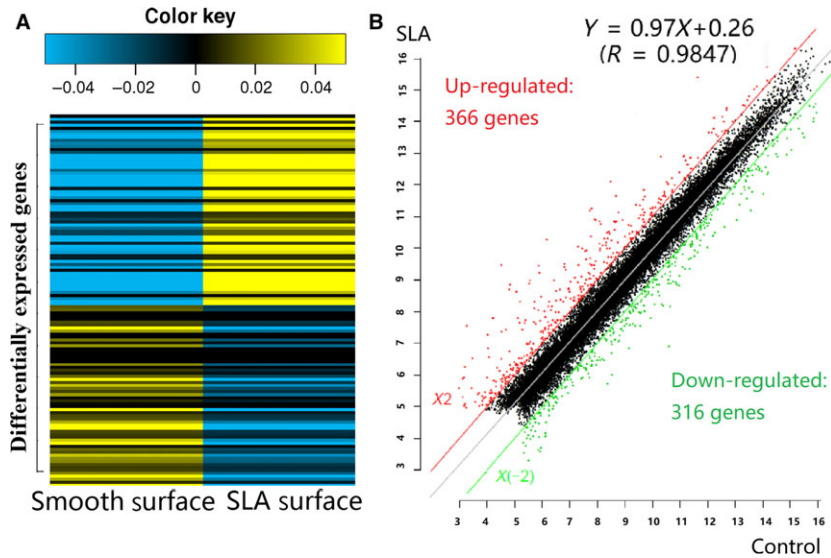


Fig. 5. Differential expression of genes in human bone marrow mesenchymal stem cells (hBMSCs) cultured on sandblasted, large-grit, acid-etched (SLA) titanium compared with hBMSCs cultured on machined smooth titanium was determined using the IncRNA & mRNA Human Gene Expression Microarray V4.0. (A) Heat map of hierarchical clustering analysis represents mRNA levels from up-regulated (yellow) to down-regulated (blue). (B) Number of up-regulated or down-regulated genes.

may account for the osteoconductive role of SLA-treated Ti implants.

The present study reveals that the rough topography of surfaces following SLA treatment induces osteogenic differentiation of hBMSCs. Microarrays and bioinformatics are useful and powerful tools employed in this report to characterize the underlying mechanism of SLA treatment on osseointegration (2, 37). To our knowledge, no genome-wide DNA-methylation profiling or association analysis between DNA methylation and mRNA expression in hBMSCs grown on Ti has been conducted. Little is known about the role of DNA methylation in the genetic mechanism of osseointegration, limiting our efforts to elucidate the genetic mechanism and develop effective treatments for implants.

In the present study, the differentially methylated sites, genes, and pathways resulting from SLA treatment were fully investigated. Epigenetic regulation of gene expression is a key mechanism that governs stemness, commitment, and differentiation (25). The data in the present study demonstrate that the methylation level of CpG sites is significantly higher in hBMSCs grown on SLA-treated Ti than in hBMSCs grown on machined smooth Ti; thus, the methylation state could be responsible for the improved osseointegration of SLA-treated surfaces. However, another study states that DNA demethylation by 5-aza-dC stimulates osteogenic differentiation of hBMSCs (38). This inconsistency can be explained by the fact that both the hypermethylation of suppressor genes and the hypomethylation of osteogenic genes contribute to osteoblast differentiation. This indicates the existence of two different mechanisms of DNA methylation-dependent gene regulation in osteogenic differentiation of hBMSCs, and SLA-treated surfaces affect suppressor

genes to a significantly greater extent than osteogenic genes.

The mean  $\beta$ -value of cg20890325 located in the promoters of *CTBP1* was significantly higher in the SLA-treated group than in the machined group. The *CTBP1* protein is a transcriptional corepressor that interacts with a variety of proteins, including Smad6 (39). A previous study demonstrated that Smad6 repressed bone morphogenetic protein (BMP)-regulated transcription of the *ID1* gene through recruiting *CTBP1* (39). Another study also indicated the negative role of *CTBP1* in osteogenesis (40). The authors of this study reported that the overexpression of *CTBP1* suppressed signaling by BMP proteins and that small interfering RNA against *CTBP1* efficiently enhanced BMP-stimulated expression of *ID1* (40). Consistently, the hypermethylation level of *CTBP1* in our study also suggested that the hypermethylation of suppressor genes contributed to the stronger osteogenic differentiation of hBMSCs in the SLA-treated group compared with the machined group.

In this study, interaction pathway analysis demonstrated that the genes of the Wnt signaling pathway were significantly differentially methylated by SLA treatment, in addition to cell adhesion molecules and proteins of the cadherin signaling pathway. The Wnt signaling pathway is a group of signal transduction pathways comprising proteins that pass signals from the outside of a cell to the inside of the cell through cell-surface receptors (2). To date, numerous studies have focused on Wnt signaling and osteogenesis (41–43). However, these studies have explored different aspects. Beta-catenin binding was also presented in the GO analysis in our study. Beta-catenin is the central factor in the canonical Wnt pathway, and the results of a previous study suggest that Wnt signals activate the

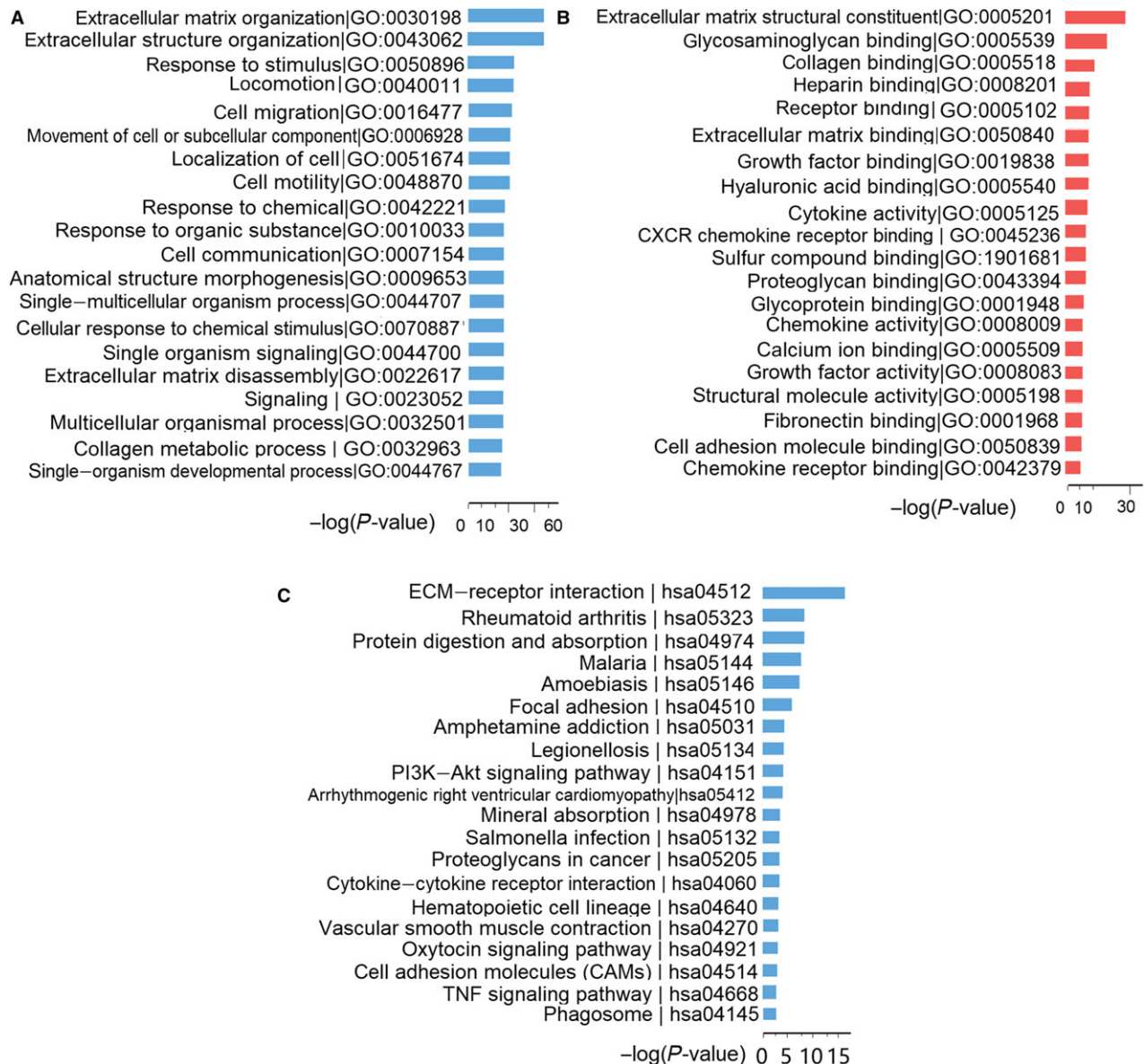


**Fig. 6.** Gene ontology (GO) analysis and KEGG pathway analysis of genes for genome-wide mRNA profiles (A) Summary of the GO analysis of the categories of 'Biological processes' among the differentially expressed genes. The GO category is listed on the y-axis. (B) Summary of the GO analysis of the categories of 'Cellular components (red)' among the differentially expressed genes. The GO category is listed on the y-axis. (C) KEGG pathway analysis of the differentially expressed genes.

$\beta$ -catenin pathway by forming oligomers containing its receptors, Frizzled and LRP (43). Furthermore, researchers note that crosstalk between the cell division cycle 42 (CDC42) protein and the Wnt/ $\beta$ -catenin pathway through glycogen synthase kinase 3 beta (GSK3b) modulates the osteogenic inductive effect of micro/nano-textured topography on rat mesenchymal stem cells (MSCs) (44). Therefore, according to our data, both the Wnt signaling pathway and  $\beta$ -catenin were involved in the osteogenesis of BMSCs on SLA-treated surfaces.

We used the lncRNA & mRNA Human Gene Expression Microarray V4.0 to characterize expression of mRNA and integrated the data obtained with DNA-

methylation data. We identified disease terms significantly enriched in the differentially methylated genes. Genes involved in type 2 diabetes and obesity-related traits were significantly enriched in the SLA-treated group. Altered bone metabolism is one of the important long-term complications associated with diabetes mellitus. Researchers report that diabetes has an important effect on immune responses, enhancing osteoclast genesis and increasing osteoblast apoptosis (45, 46). A previous study detected differentially expressed genes in bone tissues surrounding implants in diabetic rats using gene chip technology. The authors of this study found that expression of osteoblast-related genes was down-regulated in bone tissue samples from diabetic rats, and

Table 3

Significantly hypomethylated or hypermethylated CpG site of which the corresponding gene was up-regulated or down-regulated in human bone marrow mesenchymal stem cells (hBMSCs) cultured on sandblasted, large-grit, acid-etched (SLA)-treated titanium compared with a machined smooth titanium surface

Target ID	Beta-Difference	Mean SLA DNA	Mean machined DNA	P-value	Adjust P-value	UCSC REFGENE NAME
cg15508379	-0.107	0.458	0.565	0.013	0.013	<i>INS-IGF2</i>
cg09336243	0.114	0.616	0.502	0.040	0.040	<i>CPXM2</i>

The methylation level of a locus was measured as beta ( $\beta$ ) =  $M/(M + U)$ , where  $M$  was the methylated signals and  $U$  was the unmethylated signals. For a gene corresponding to a CpG site, Mean SLA DNA and Mean machined DNA represent the  $\beta$  value of SLA group and machined smooth group, respectively. Beta-Difference equals the  $\beta$  value differences between the SLA group and the machined smooth group. For multiple testing the Adjust  $P$  value was corrected by Benjamini-Hochberg tests at 5% false discovery rate (FDR). UCSC REFGENE NAME represents the gene symbol corresponding to the CpG site.

The CpG sites with both adjusted  $P \leq 0.05$  and  $|\beta$  difference|  $\geq 0.10$  were identified as significantly differentially methylated loci. *CPXM2*, carboxypeptidase X, M14 Family Member 2; *INS-IGF2*, INS-IGF2 readthrough.

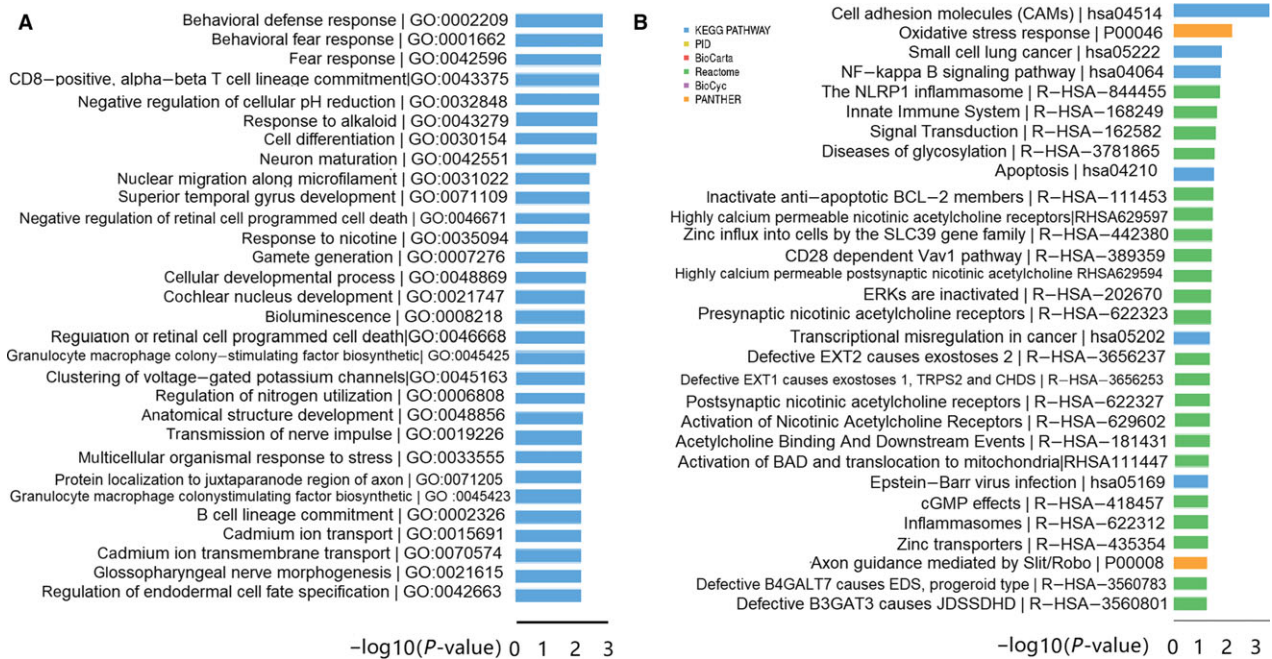


Fig. 7. Gene ontology (GO) analysis and KEGG pathway analysis of genes integrating mRNA expression and DNA methylation data. (A) Enriched GO terms for the detected genes integrating mRNA expression and DNA methylation data in the categories of 'Biological processes' among the differentially expressed genes. The GO category is listed on the y-axis. (B) KEGG pathway analysis of the genes integrating mRNA expression and DNA methylation data.

the lipid metabolism pathway was up-regulated (47). This suggests that diabetes and obesity may be risk factors of implant surgery and decrease osteointegration, while patients with diabetes or obesity may benefit from an SLA-treated implant.

We identified 37 genes that had a negative association between methylated CpG sites and mRNA expression. Among these genes, the level of insulin-like growth factor 2 (*IGF2*) mRNA was up-regulated, corresponding to the most significantly hypomethylated CpG site. A previous study suggested that IGF2 plays an important role in bone formation in osteoblasts and in the differentiation progress of BMSCs to osteoblasts (48). So, the hypomethylation of *IGF2* may contribute to the better

osteogenic differentiation of hBMSCs in the SLA-treated group compared with the machined group. Similarly, *CPXM2* was also hypermethylated in our study. The *CPXM2* gene is downregulated and involved in ECM organization in Apert syndrome, which involves increased potential for bone differentiation (49).

In conclusion, the present study characterizes the DNA-methylation profiles of hBMSCs on SLA-treated and smooth Ti surfaces using Illumina 850 K Methylation Bead Chip. The genes and pathways identified may participate in the osteoblast differentiation and osseointegration on Ti surfaces. These genes may be used to enhance the osteogenic ability of hBMSCs on SLA-treated surfaces through epigenetic strategies.

However, further studies are needed to investigate the underlying mechanism.

**Acknowledgement** – This study was financially supported by grants from the National Natural Science Foundation of China (No. 81771106) and the National Key R&D Program of China (2016YFC1102705). Authors Mingyue Lyu and Yunfei Zheng contributed equally to this work.

**Conflicts of interest** – The paper is original and free of any conflict of interest.

## References

- DONOS N, HAMLET S, LANG NP, SALVI GE, HUYNH-BA G, BOSSHARDT DD, IVANOVSKI S. Gene expression profile of osseointegration of a hydrophilic compared with a hydrophobic microrough implant surface. *Clin Oral Implants Res* 2011; **22**: 365–372.
- YANG G, FANG W, LIU T, HE F, CHEN X, ZHOU Y, GUAN X. Gene expression profiling of bone marrow-derived stromal cells seeded onto a sandblasted, large-grit, acid-etched-treated titanium implant surface: the role of the Wnt pathway. *Arch Oral Biol* 2016; **61**: 71–78.
- LI J, WEI Q, ZHANG K, FENG W, PING Y, HE Z, ZHAO A, NAN H. Controlling mesenchymal stem cells differentiate into contractile smooth muscle cells on a TiO<sub>2</sub> micro/nano interface: towards benign pericytes environment for endothelialization. *Colloids Surf B Biointerfaces* 2016; **145**: 410.
- SABRINA P, RAJESH P, WEBSTER TJ. Nano rough micron patterned titanium for directing osteoblast morphology and adhesion. *Int J Nanomedicine* 2008; **3**: 229.
- KLEIN MO, BIJELIC A, ZIEBART T, KOCH F. Submicron scale-structured hydrophilic titanium surfaces promote early osteogenic gene response for cell adhesion and cell differentiation. *Clin Implant Dent Relat Res* 2013; **15**: 166–175.
- BARFEIE A, WILSON J, REES J. Implant surface characteristics and their effect on osseointegration. *Br Dent J* 2015; **218**: E9.
- COCHRAN DL, JACKSON JM, BERNARD JP, TEN BRUGGENKATE CM, BUSER D, TAYLOR TD, WEINGART D, SCHOOLFIELD JD, JONES AA, OATES TW Jr. A 5-year prospective multicenter study of early loaded titanium implants with a sandblasted and acid-etched surface. *Int J Oral Maxillofac Implants* 2011; **26**: 1324–1332.
- GUEHENNEC LL, LAYROLLE AS, AMOURIQ Y. Surface treatments of titanium dental implants for rapid osseointegration. *Dent Mater* 2007; **23**: 844–854.
- BRETT PM, HARLE J, SALIH V, MIHOC R, OLSEN I, JONES FH, TONETTI M. Roughness response genes in osteoblasts. *Bone* 2004; **35**: 124–133.
- COCHRAN DL, NUMMIKOSKI PV, HIGGINBOTTOM FL, HERMANN JS, MAKINS SR, BUSER D. Evaluation of an endosseous titanium implant with a sandblasted and acid-etched surface in the canine mandible: radiographic results. *Clin Oral Implants Res* 1996; **7**: 240–252.
- LI D, FERGUSON SJ, BEUTLER T, COCHRAN DL, SITTIG C, HIRT HP, BUSER D. Biomechanical comparison of the sandblasted and acid-etched and the machined and acid-etched titanium surface for dental implants. *J Biomed Mater Res* 2002; **60**: 325–332.
- WENNERBERG A, ALBREKTSSON T. Effects of titanium surface topography on bone integration: a systematic review. *Clin Oral Implants Res* 2009; **20**: 172–184.
- BUSER D, NYDEGGER T, OXLAND T, COCHRAN DL, SCHENK RK, HIRT HP, SNĚTIVY D, NOLTE LP. Interface shear strength of titanium implants with a sandblasted and acid-etched surface: a biomechanical study in the maxilla of miniature pigs. *J Biomed Mater Res* 1999; **45**: 75–83.
- GERMANIER Y, TOSATTI S, BROGGINI N, TEXTOR M, BUSER D. Enhanced bone apposition around biofunctionalized sandblasted and acid-etched titanium implant surfaces. A histomorphometric study in miniature pigs. *Clin Oral Implants Res* 2006; **17**: 251–257.
- BIANCO P, ROBEY PG, SIMMONS PJ. Mesenchymal stem cells: revisiting history, concepts, and assays. *Cell Stem Cell* 2008; **2**: 313–319.
- KHAN MR, DONOS N, SALIH V, BRETT M. The enhanced modulation of key bone matrix components by modified Titanium implant surfaces[J]. *Bone* 2012; **50**: 1–8.
- YI TG, HYUN-JOO L, YUN-KYOUNG C, MYUNG-SHIN J, SONG SU. Molecular characterization of neurally differentiated human bone marrow-derived clonal mesenchymal stem cells. *Immune Netw* 2014; **14**: 54–65.
- ZHANG Z, XIE Y, PAN H, HUANG L, ZHENG X. Influence of patterned titanium coatings on polarization of macrophage and osteogenic differentiation of bone marrow stem cells. *J Biomater Appl* 2018; **32**: 97.
- WEI Y, CHEN YH, LI LY, LANG J, YEH SP, SHI B, YANG CC, YANG JY, LIN CY, LAI CC. CDK1-dependent phosphorylation of EZH2 suppresses methylation of H3K27 and promotes osteogenic differentiation of human mesenchymal stem cells. *Nat Cell Biol* 2011; **13**: 87–94.
- SCHILLER M, JAVELAUD D, MAUVIEL A. TGF-beta-induced SMAD signaling and gene regulation: consequences for extracellular matrix remodeling and wound healing. *J Dermatol Sci* 2004; **35**: 83–92.
- SUZUKI MM, BIRD A. DNA methylation landscapes: provocative insights from epigenomics. *Nat Rev Genet* 2008; **9**: 465.
- GIL-CAYUELA C, ROSELLO LE, TARAZON E, ORTEGA A, SANDOVAL J, MARTINEZ-DOLZ L, CINCA J, JORGE E, GONZALEZ-JUANATEY JR, LAGO F, RIVERA M, PORTOLES M. Thyroid hormone biosynthesis machinery is altered in the ischemic myocardium: an epigenomic study. *Int J Cardiol* 2017; **243**: 27–33.
- JAENISCH R, BIRD A. Epigenetic regulation of gene expression: how the genome integrates intrinsic and environmental signals. *Nat Genet* 2003; **33**: 245.
- AI T, TINGTING A, JIENI Z, XUEDONG W, XIAOWEN Z. DNA methylation profile is associated with the osteogenic potential of three distinct human odontogenic stem cells. *Signal Transduct Target Ther* 2018; **3**: 1–8.
- HE W, KANG X, DU H, SONG B, LU Z, HUANG Y, WANG D, SUN X, YU Y, FAN Y. Defining differentially methylated regions specific for the acquisition of pluripotency and maintenance in human pluripotent stem cells via microarray. *PLoS ONE* 2014; **9**: e108350.
- TESCHENDORFF AE, MARABITA F, LECHNER M, BARTLETT T, TEGNER J, GOMEZ-CABRERO D, BECK S. A beta-mixture quantile normalization method for correcting probe design bias in Illumina Infinium 450 k DNA methylation data. *Bioinformatics* 2013; **29**: 189–196.
- PAN H, CHEN L, DOGRA S, TEH AL, TAN JH, LIM YI, LIM YC, JIN S, LEE YK, NG PY. Measuring the methylome in clinical samples: improved processing of the Infinium Human Methylation450 BeadChip Array. *Epigenetics* 2012; **7**: 1173–1187.
- HUANG J, ZHANG X, YAN W, CHEN Z, SHUAI X, WANG A, YAN W. Nanotubular topography enhances the bioactivity of titanium implants. *Nanomedicine* 2017; **13**: 1913.
- DU P, KIBBE WA, LIN SM. lumi: a pipeline for processing Illumina microarray. *Bioinformatics* 2008; **24**: 1547–1548.
- YAN H, GUAN Q, HE J, LIN Y, ZHANG J, LI H, LIU H, GU Y, GUO Z, HE F. Individualized analysis reveals CpG sites with methylation aberrations in almost all lung adenocarcinoma tissues. *J Transl Med* 2017; **15**: 26.
- BUSER D. Implants in the atrophic partially edentulous maxilla. Single tooth gaps vs extended edentulous spaces. *Int J Oral Maxillofac Implants* 2003; **18**: 761.
- KIESWETTER K, SCHWARTZ Z, HUMMERT TW, COCHRAN DL, SIMPSON J, DEAN DD, BOYAN BD. Surface roughness modulates the local production of growth factors and cytokines by osteoblast-like MG-63 cells. *J Biomed Mater Res* 1996; **32**: 55–63.
- LV L, LIU Y, ZHANG P, ZHANG X, LIU J, CHEN T, SU P, LI H, ZHOU Y. The nanoscale geometry of TiO<sub>2</sub> nanotubes influences the osteogenic differentiation of human adipose-

- derived stem cells by modulating H3K4 trimethylation. *Bio-materials* 2015; **39**: 193–205.
34. SCHIEGNITZ E, PALARIE V, NACU V, AL-NAWAS B, KÄMMERER PW. Vertical osteoconductive characteristics of titanium implants with calcium-phosphate-coated surfaces – a pilot study in rabbits. *Clin Implant Dent Relat Res* 2014; **16**: 194–201.
  35. SIMON TM, SICKLE DCV, KUNISHIMA DH, JACKSON DW. Cambium cell stimulation from surgical release of the periosteum. *J Orthop Res* 2010; **21**: 470–480.
  36. KÄMMERER PW, GABRIEL M, ALNAWAS B, SCHOLZ T, KIRCHMAIER CM, KLEIN MO. Early implant healing: promotion of platelet activation and cytokine release by topographical, chemical and biomimetic titanium surface modifications in vitro. *Clin Oral Implants Res* 2012; **23**: 504–510.
  37. SILVA HF, ABUNA RPF, LOPES HB, FRANCISCHINI MS, DE OLIVEIRA PT, ROSA AL, BELOTI MM. Participation of extracellular signal-regulated kinases 1/2 in osteoblast and adipocyte differentiation of mesenchymal stem cells grown on titanium surfaces. *Eur J Oral Sci* 2017; **125**: 355–360.
  38. EL-SERAFI AT, OREFFO R, ROACH H. The DNA methylation inhibitor 5-aza-deoxycytidine enhances osteogenic differentiation of human skeletal stem cells: epigenetic approaches to bone tissue regeneration. *Bone* 2010; **47**: S120.
  39. LIN X, LIANG YY, SUN B, LIANG M, SHI Y, BRUNICARDI FC, SHI Y, FENG XH. Smad6 recruits transcription corepressor CtBP to repress bone morphogenetic protein-induced transcription. *Mol Cell Biol* 2003; **23**: 9081–9093.
  40. WU X, CHANG MS, MITSIALIS SA, KOUREMBANAS S. Hypoxia regulates bone morphogenetic protein signaling through C-terminal-binding protein 1. *Circ Res* 2006; **99**: 240.
  41. WAN Y, LU C, CAO J, ZHOU R, YAO Y, YU J, ZHANG L, ZHAO H, LI H, ZHAO J. Osteoblastic Wnts differentially regulate bone remodeling and the maintenance of bone marrow mesenchymal stem cells. *Bone* 2013; **55**: 258–267.
  42. CAI Y, CAI T, CHEN Y. Wnt pathway in osteosarcoma, from oncogenic to therapeutic. *J Cell Biochem* 2014; **115**: 625–631.
  43. CONG F, SCHWEIZER L, VARMUS H. Wnt signals across the plasma membrane to activate the beta-catenin pathway by forming oligomers containing its receptors, Frizzled and LRP. *Development* 2004; **131**: 5103–5115.
  44. LI G, SONG Y, SHI M, DU Y, WEI W, ZHANG Y. Mechanisms of Cdc42-mediated rat MSC differentiation on micro/nano-textured topography. *Acta Biomater* 2017; **49**: 235–246.
  45. WU YY, XIAO E, GRAVES DT. Diabetes mellitus related bone metabolism and periodontal disease. *Int J Oral Sci* 2015; **7**: 63–72.
  46. NIKOLAJCZYK BS, JAGANNATHAN-BOGDAN M, SHIN H, GYURKO R. State of the union between metabolism and the immune system in type 2 diabetes. *Genes Immun* 2011; **12**: 239–250.
  47. WANG XX, MA Y, LI Q, JIANG BQ, LAN J. Differential expression genes of bone tissues surrounding implants in diabetic rats by gene chip. *Shanghai Kou Qiang Yi Xue* 2012; **21**: 521.
  48. OSAKA T, ABIKO Y. IGF-II and IGFBP-2 gene expressions responsible for osteoblastic differentiation from human bone marrow derived mesenchymal stem cells. *J Ultrastruct Res* 1970; **31**: 439–443.
  49. ÇETINKAYA A, TAŞKIRAN E, SOYER T, ŞİMŞEK-KİPER PÖ, ÜTİNE GE, TUNÇBILEK G, BODUROĞLU K, ALIKAŞIYOĞLU M. Dermal fibroblast transcriptome indicates contribution of WNT signaling pathways in the pathogenesis of Apert syndrome. *Turk J Pediatr* 2017; **59**: 619.